Communication

Israel Journal of Chemistry

DOI: 10.1002/ijch.202000098

Benzothiazole-Phenothiazine Conjugate Based Molecular Probe for the Differential Detection of Glycated Albumin

Ashish Kumar[+],[a] Lakshmi Priya Datta[+],[a] Sourav Samanta[+],[a] Harshit Arora,[a] and Thimmaiah Govindaraju*[a]

Abstract: Glycation of albumin proteins is considered the pathophysiological hallmark of several chronic fatal disorders, including diabetes mellitus (DM) and Alzheimer's disease (AD). The optical detection of glycated albumin is a simple and cost-effective tool with diagnostic implications for DM and AD. Herein, we developed a cyano derivative of the benzothiazole-phenothiazine conjugate ($T_{CN}P$) -based far-red fluorescence probe for the differential detection of glycated bovine serum albumin (BSA_G) over native BSA and oxidized BSA (BSA_O). The selective fluorescence enhancement of $T_{CN}P$ in the presence of native BSA and BSA_O and significant quenching in the presence of BSA_G account for the distinct interaction between the probe and different structural variants of BSA. The high photostability and differential response towards native BSA and BSA_G infer that $T_{CN}P$ is a potential molecular tool to assess the glycation induced structural changes of albumins.

Keywords: Albumin · Oxidation · Glycation · Far-red Fluorescence Probe · Differential Detection

DM is considered one of the most prevalent metabolic disorders affecting more than 415 million individuals globally, and the number of cases is estimated to cross over 642 million by 2040.[1,2] The dreadful nature of DM is associated with several neurological disorders like AD. DM triggers the development of AD by promoting the blood-brain barrier damage,[3,4] leading to the accumulation of misfolded amyloid β (Aβ) peptides in the AD brain and related toxicities.[5–8] The complications and evidence of DM link in neuropathological diseases have led researchers to monitor blood glucose levels critically. Quantitative determination of glycated proteins, especially glycated hemoglobin A1c (HbA1c), is considered one of the potential tools to detect hyperglycemia.[9] However, the analysis has limitations regarding the use of HbA1c as a short-term regular glycemic control.[10,11] The serum albumin proteins (BSA: bovine serum albumin and HSA: human serum albumin) account for ~50% of the total blood protein content and exhibit several biomechanical properties, including oncotic pressure maintenance,[12,13] metal chelation,[14] interaction with biomolecular entities,[15,16] transport of both endogenous as well as exogenous cargo ligands, and immunomodulation.[17] The remarkable ligand-binding features of albumin proteins are attributed to undergoing glycation at multiple sites, which is of significant interest to researchers and clinicians as a credible indicator of serum blood glucose level.[18,19] The nonenzymatic glycations of those albumin proteins are a type of post-translational modifications where the nucleophilic addition of reducing sugars to the free amine or carbonyl groups of proteins forms reversible Schiff base intermediate which rearranges to form the Amadori products and further rearrangements like oxidation or cyclization trigger formation of advanced glycated end products (AGEs).[20] The serum albumin proteins of the native BSA consisting of 583 amino acids with 67% helix, 10% turn, and 23% extended chain configuration with 17 disulfide bridges form a triple-domain conformation.[21] The secondary structure of BSA is vital to maintain the structure-function relationship and the aberrant structural changes are implicated in various pathological conditions (Figure 1A). In addition to glycation, BSA undergoes substantial structural changes upon oxidation (BSA_O).[22] The formation of BSA_O from native BSA triggers the accumulation of reactive oxygen species (ROS) under pathological conditions in the body and a critical indication of oxidative stress, which is linked with disease conditions of DM, age-related disorders, and neurological disorders.[23–26] The nonenzymatic glycation of BSA is an inevitable repercussion of increased blood glucose levels under the DM conditions, potentially facilitating the formation of heterogeneous AGEs. The AGE-associated structural changes promote the formation of neurofibrillary tangles (NFT) and amyloid plaques, eventually leading to AD development.[24,27] In this context, selective detection of different structural variants of BSA is of foremost importance from the clinical perspective. The conventional methods for detecting glycated proteins, including glycated hemoglobin and albumin, are based on various chromatography, electrochemistry, and immunochemistry techniques.[12,28–30] In the recent past, advanced immuno-

[a] *A. Kumar,[+] Dr. L. P. Datta,[+] S. Samanta,[+] H. Arora, Prof. T. Govindaraju*
Bioorganic Chemistry Laboratory, New Chemistry Unit and The School of Advanced Materials (SAMat), Jawaharlal Nehru Centre for Advanced Scientific Research (JNCASR), Jakkur P. O., Bengaluru-560064, Karnataka, India
E-mail: tgraju@jncasr.ac.in

[+] *Equal first authorship (contributed equally to this work)*

Supporting information for this article is available on the WWW under https://doi.org/10.1002/ijch.202000098.

Israel Journal of Chemistry

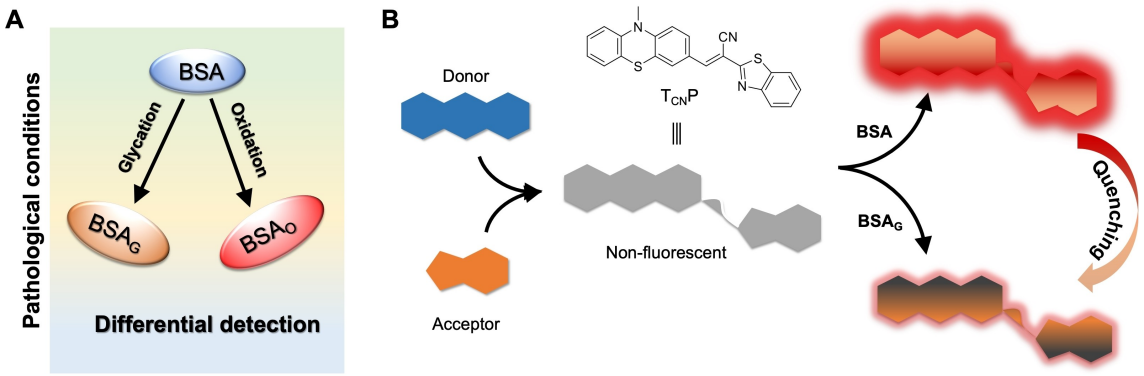

Figure 1. (**A**) Schematic representation of BSA and its structural variants as pathophysiological markers. (**B**) The design strategy of D-π-A architecture based far-red fluorescence probe ($T_{CN}P$) and its application in the differential detection of different structural variants of BSA.

assay sensory platform,[31] enzymatic assay,[32] and electroluminescence[33] based techniques have been reported for the detection of glycated albumins. For bio-analyte detection, the optical methods and assays are considered advantageous due to their simple design, ease of handling, low cost, and rapid quantification ability.[34] In practice, bio-analyte responsive far-red fluorescent probes can outweigh visible fluorescence probes for *in vitro* and *in vivo* applications, as they cause minimal photodamage to the samples, exhibit intense tissue penetration ability, and circumvent the problem of autofluorescence from the surroundings.[35] In this aspect, the tailored design of far-red (650 nm–900 nm) fluorescence probes for the detection of various biological analytes and markers have gained considerable attention from the scientific community.[36–46] For *in vivo* applications, laser light source for excitation and two-photon microscopy techniques will be useful. While a range of fluorescence probes have been reported for the detection of BSA or HSA,[36,47,48] far-red fluorescence probe for the selective and differential detection of structural variants of BSA has not been documented. For instance, the extent of glycation and oxidation of BSA are found to be elevated in DM patients, and these structural alterations significantly impair the inherent binding affinity of BSA to a range of external ligands, including drugs and probes.[49,50] The conformational changes modify the three-dimensional structure and make the ligand binding cavities (site I and site II) narrow and shallow with leading to compromised accessibility. Therefore, designing fluorescence probes to differentially interact with the glycated albumin by sensing the structural changes is challenging.

In this work, we designed a far-red donor-π-acceptor (D-π-A) system-based benzothiazole-phenothiazine probe ($T_{CN}P$) for the differential detection of structural variants of BSA. The photostability of fluorescent probes is a primary determinant for its practical utility. Incorporation of cyano group in the bridge (vinyl linkage) of donor and acceptor moieties was considered in our probe design.[51] This electron-withdrawing cyano group suppresses the oxidative photo-bleaching and significantly improve the photostability and applicability of the probe ($T_{CN}P$).[51–53] It has been established that the cyano group substantially prevents the dye degradation from singlet oxygen species[53] and a beneficial strategy to improve the photostability. Incorporation of electron-withdrawing cyano group in the design strategy influences the energy difference profile between the highest occupied molecular orbital (HOMO) and lowest unoccupied molecular orbital (LUMO) of $T_{CN}P$ that triggers the far-red emission along with improving the photostability. The probe was synthesized by conjugating N-methyl phenothiazine (electron-donor, D) with 2-(cyanobenzothiazol-2-yl) acetonitrile (electron-acceptor, A) moiety through a vinyl linkage (π-linker unit) employing Knoevenagel-type condensation. The phenothiazine was treated with sodium hydride (NaH) under ice-cold condition followed by addition of methyl iodide (MeI) and the reaction mixture was heated at 40 °C to obtain 10-methyl-10H-phenothiazine (**1**) (Scheme S1). The intermediate **1** was treated with phosphonium oxychloride ($POCl_3$) in DMF under heating conditions to obtain 10-methyl-10H-phenothiazine-3-carbaldehyde (**2**). Finally, the intermediate **2** was condensed with 2-(cyanobenzothiazol-2-yl) acetonitrile by Knoevenagel-type condensation in the presence of an organic base to obtain the desired product $T_{CN}P$ as an orange-red solid. All the intermediates and the final product were characterized by NMR and HRMS analysis. The D-π-A molecular system $T_{CN}P$, exhibits a weak fluorescence signal in phosphate buffer saline (PBS: 10 mM, pH = 7.4) with $\lambda_{max} = 672$ nm upon excitation at 480 nm (Figure S1). The observed spectral behavior is particularly interesting from the perspective of an ideal fluorescent molecular sensor (non-fluorescent in free-state and strongly fluorescent in the analyte bound-state) (Figure 1).[36,54,55] The weakly fluorescent $T_{CN}P$ show turn-on emission in the presence of BSA. $T_{CN}P$ was found to selectively detect BSA in mixed samples consisting of various biological analytes. Subsequently, the detection of different structural variants of BSA (BSA_O and BSA_G) was considered. The differential sensing ability of $T_{CN}P$ towards BSA variants was monitored through a series of spectroscopy measurements.

The photophysical properties of fluorescent probe $T_{CN}P$ are interesting due to the presence of donor and acceptor units linked through the π-bridge, which is responsible for the formation of an internal charge transfer (ICT) state in the polar environment.[39] The probability of forming an ICT state and response of $T_{CN}P$ towards different solvent systems was assessed by recording the absorbance and fluorescence spectra in solvents of varying polarity (Figure S2A and S2B). The data showed a gradual shifting of absorption (λ_{max} = 464 nm in toluene to 484 nm in PBS) and emission (λ_{em} = 628 nm in toluene to 672 nm in PBS) maxima towards longer wavelength regions accompanied by the reduction in emission intensity with increasing solvent polarity from toluene to PBS. The observed bathochromic shift in polar solvents accounts for the stabilization of the excited state and photoinduced ICT. The observed data can be explained by the Lippert-Mataga theory (effect of solvent polarity on fluorophore), which provides a definitive approach to analyze the photophysical data of the probe in solvents of varying polarity.[56] The mathematical expression of the Lippert-Mataga equation is as follows:

$$\mathbf{v_A} - \mathbf{v_B} = \frac{2}{\mathbf{hc}} \frac{\left(\varepsilon - 1/2\varepsilon + 1 - \mathbf{n}^2 - 1/2\,\mathbf{n}^2 + 1\right)(\mu_E - \mu_G)^2}{\mathbf{a}^3}$$

where, *h* is the Planck's constant, c is the speed of light, *a* is the radius of the cavity in which the fluorophore resides, n is the refractive index of the solvent, and ε is the dielectric constant of the solvent, ν_A, and ν_F are the wavenumbers (cm^{-1}) of absorption and fluorescence, and μ_E and μ_G correspond to the dipole moments of the probe in the respective ground and excited states. The change in the spectral shifts is verified by analyzing the reorientation of solvents upon interaction with the probe molecule, which is termed as orientation polarizability [Δf(ε,n)] and expressed by the mathematical formula,

$$[\Delta f(\varepsilon, n)] = \left(\varepsilon - 1/2\varepsilon + 1 - \mathbf{n}^2 - 1/2\,\mathbf{n}^2 + 1\right)$$

The non-linear Lippert plot validates specific interaction between $T_{CN}P$ and solvents of different polarity, and the change in energy of the fluorophore is dependent on the dielectric constant of the medium (Figure S3). The photostability of the probe was investigated by irradiating $T_{CN}P$ (10 μM, PBS:DMSO, 1 : 1, v/v) with a 100 W high power light source. The negligible changes in the absorbance intensity upon irradiation for 1 h confirmed the excellent photostability of $T_{CN}P$ (Figure S4). The observed photostability of the probe $T_{CN}P$ reinforced the design strategy of incorporating cyano-group in the probe. Further, we investigated the stability of $T_{CN}P$ in different external physical and chemical conditions such as temperature, pH, and in the presence of various reactive oxygen species (ROS). To assess the thermal stability, we recorded the fluorescent spectra of $T_{CN}P$ (10 μM) in PBS over the temperature range of 20–80 °C upon exciting at 480 nm. The emission spectra at different temperatures showed minimal changes confirming the thermal stability of $T_{CN}P$ (Figure S5). We incubated $T_{CN}P$ (10 μM) in solutions of varying pH (1 to 13) for 10 min, and the fluorescent spectra were recorded. The $T_{CN}P$ fluorescence did not change significantly over a broad pH range, which confirmed pH stability of the probe and its suitability under the physiological conditions (Figure S6). Under extreme physical (temperature) and chemical (pH) stimuli, viz., above 70 °C and below pH 2, marginal reduction in the basal fluorescence of $T_{CN}P$ was observed. These are mostly outside the biologically relevant conditions and not expected to affect the utility of the probe. The cellular oxidative stress is a common phenomenon under disease conditions, and it is essential to investigate the fate of $T_{CN}P$ under these conditions. We recorded fluorescence spectra of $T_{CN}P$ in the presence of different ROS (H_2O_2, $HO^{\bullet}$, NO_2^-, NO_3^- and ClO^-). For the experiment, $T_{CN}P$ (10 μM) was incubated with ROS (50 μM) in PBS (10 mM, pH = 7.4) for 10 min, and the $T_{CN}P$ emission was monitored upon excitation at 480 nm. Interestingly, the $T_{CN}P$ emission remained mostly unaffected by ROS at their high concentrations, which affirmed the suitability of the probe for practical applications under cellular conditions (Figure S7).

Next, the utility of $T_{CN}P$ as a molecular probe to sense the albumins was evaluated. The structural homology between BSA and HSA makes them identical in terms of ligand binding ability. The selectivity of the probe $T_{CN}P$ towards BSA and HSA was investigated in comparison with other biological analytes such as trypsin, glutathione, and skimmed milk. The fluorescence spectra were recorded by exciting $T_{CN}P$ (10 μM) at 480 nm in PBS buffer and maintaining the stoichiometric ratio of probe:analyte at 1 : 1 (Figure 2A). $T_{CN}P$ showed a hypsochromic shift (~55 nm) in its fluorescence maxima (λ_{max} = 672 nm) upon interaction with BSA or HSA. A significant enhancement in the fluorescence emission intensity (~7- and 6-fold increment for BSA and HSA, respectively) was also observed. While, negligible changes in the fluorescence emission intensity of $T_{CN}P$ in the presence of trypsin and glutathione were observed, which revealed the selectivity of the probe towards albumins. Notably, the slight fluorescence response of the probe observed for skimmed milk is attributed to the presence of albumin proteins. The crystal structure analysis of BSA and HSA protein revealed three different drug-binding domains (domains I, II, and III), and the drug molecules generally bind to the sudlow 1 and sudlow 2 sites present in domain II and III.[57,58]

The sudlow site I is known for the entrapment of hydrophobic drugs within its large hydrophobic cavity, and the hydrophobic nature of $T_{CN}P$ accounts for its potential binding in sudlow site I.[36] The fluorescence titration experiment was performed to gain insight into the binding interactions between BSA and $T_{CN}P$. Increasing concentrations of BSA (0–900 μM) were titrated against a fixed concentration of the probe $T_{CN}P$ (10 μM), and the changes in fluorescence emission intensity at 619 nm was monitored upon excitation at 480 nm (Figure 2B). With BSA titration, the λ_{max} value of the probe shifted towards a lower wavelength accompanied by the gradual increase in

Israel Journal of Chemistry

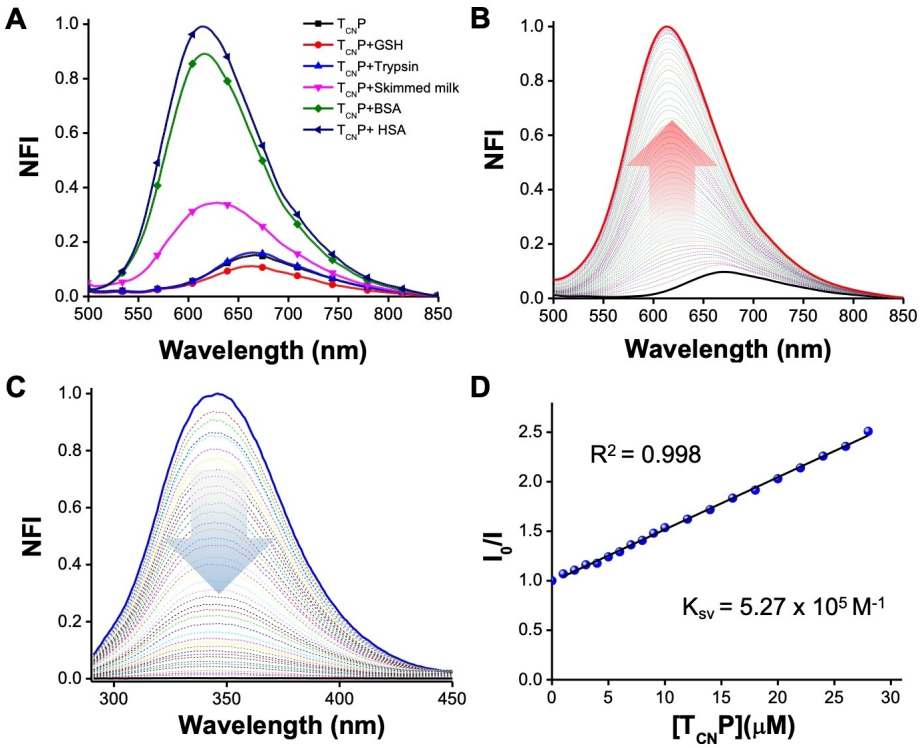

Figure 2. (**A**) Selective detection of albumins (HSA and BSA) by $T_{CN}P$ (λ_{ex} = 480 nm λ_{em} = 619 nm) over other biological analytes (trypsin, GSH, skimmed milk). **(B)** The change in emission spectra of $T_{CN}P$ (10 μM) upon addition of increasing concentration of BSA (0–900 μM). **(C)** The change in intrinsic fluorescence of BSA (10 μM) (λ_{ex} = 278 nm, λ_{em} = 340 nm) with increasing concentration of $T_{CN}P$ (0–700 μM) and (**D**) the corresponding Stern-Volmer plot of intrinsic fluorescence change of BSA with increasing concentration of $T_{CN}P$ to calculate K_{sv} (quenching constant). NFI: Normalized fluorescence intensity.

the emission intensity. The enhancement in emission intensity and hypsochromic shift in the emission maxima validates the confinement of the probe in one of the hydrophobic pockets of BSA. The entrapment of $T_{CN}P$ within the hydrophobic cavity of BSA is anticipated to influence the conformation of the protein and potentially alter the protein microenvironment. The detailed information on the structural changes can be obtained by examining the intrinsic fluorescence at 340 nm, which corresponds to the characteristic signal of tryptophan units of BSA. BSA (10 μM) was titrated with the increasing concentration of $T_{CN}P$ (0–700 μM), and the change in the fluorescence was measured at 340 nm (λ_{ex} = 278 nm). The increasing concentrations of $T_{CN}P$ showed a gradual decrease in the fluorescence emission intensity at 340 nm, indicating possible changes in the microenvironment of aromatic residues of BSA upon binding with $T_{CN}P$ (Figure 2C). In most of the cases, upon interaction with external chemical probes, proteins get denatured, which is validated by the distinct hyperchromic shift of emission maxima at the tryptophan region.[59] However, the absence of any characteristic shift in the intrinsic fluorescence band (λ_{ex} = 340 nm) confirmed that the interaction of $T_{CN}P$ with BSA does not cause the unfolding or denaturation of the protein. The Stern-Volmer plot investigated the fluorescence quenching data, and the extent of quenching was quantified by the following equation 2.

$$I_0/I = 1 + K_q\tau_q[Q] = 1 + K_{SV}[Q]$$

Where, I_0 and I are the steady-state fluorescence intensities in the absence and presence of quencher, respectively, K_{SV} is the Stern-Volmer quenching constant, τ_q is the average lifetime of the protein without the quencher, and [Q] is the concentration of the quencher ($T_{CN}P$). The K_{SV} value was determined by plotting I_0/I at 340 nm against the probe concentration (Figure 2D) and was found to be 5.26×10^5 M^{-1} as measured by the linear regression assessment, which ensures effective interaction between BSA and $T_{CN}P$. BSA_O accounts for several pathological conditions in the body,[60] and investigating the ability of the probe to interact with BSA_O is of great interest. To assess the interaction, the native BSA was subjected to oxidation by incubating BSA (10 μM) with hydrogen peroxide (H_2O_2, 100 μM), ferrous sulfate ($FeSO_4$, 10 μM) and EDTA (10 μM) in PBS at room temperature in the dark. The oxidation was monitored by the spectral change and cyclic voltammetric analysis. As observed from the fluorescence spectroscopy data, the emission band of BSA corresponds to the tryptophan fluorescence (λ_{em} = 340 nm, λ_{ex} = 278 nm) significantly reduced indicating the changes in the microenvironment of the tryptophan region upon oxidation (Figure 3A). Cyclic voltammetry analysis confirmed the oxidation

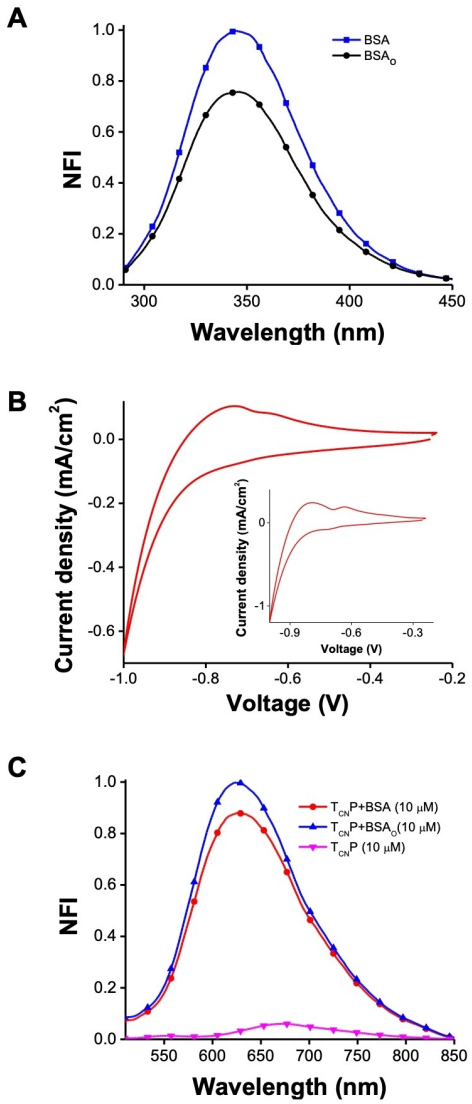

Figure 3. (**A**) The characteristic changes in intrinsic fluorescence of BSA upon oxidation (λ_{ex} = 278 nm λ_{max} = 340 nm). (**B**) Cyclic voltammetry analysis to assess the changes in current density of BSA (inset) upon oxidation (BSA$_O$). (**C**) Emission spectra of $T_{CN}P$ with native BSA and BSA$_O$ in PBS (λ_{ex} = 480 nm λ_{em} = 619 nm). NFI: Normalized fluorescence intensity.

of BSA. The native BSA showed a characteristic oxidation peak at −0.63 V and the less intense reduction peak at −0.70 V for electrochemical oxidation and reduction cycles, respectively (Figure 3B inset). However, BSA$_O$ showed a broad maximum in the range of −0.65 to −0.61 V for the oxidation, while no peak was observed for the reduction (Figure 3B). In general, the disulfide bridges of BSA are susceptible to oxidation, and the reduction leading to a possible rearrangement of the disulfide bonds of BSA. In the case of BSA$_O$, the absence of any reduction peaks indicates the complete oxidation of BSA. Next, we monitored the interaction of $T_{CN}P$ with BSA$_O$ by spectrophotometry method. As discussed (*vide supra*), $T_{CN}P$ exhibits fluorescence response with BSA, and we were intended to understand the probe response to BSA$_O$ in comparison to native BSA. $T_{CN}P$ (10 μM) was treated with BSA or BSA$_O$ (10 μM) in PBS at room temperature for 15 min, and emission spectra were recorded upon excitation at 480 nm. The data showed that the emission intensity of $T_{CN}P$ in the presence of BSA$_O$ is significantly higher compared to native BSA (Figure 3C), suggesting that $T_{CN}P$ differentially interacts with BSA and BSA$_O$. The observed photophysical changes revealed that $T_{CN}P$ exhibits moderate differential sensing ability to detect BSA$_O$ over native BSA.

As discussed earlier, BSA$_G$ is a biomarker for DM and provides information on the average glucose level in the blood.[61] As an endogenous glycemic control, the differential detection of BSA$_G$ by $T_{CN}P$ can be an important diagnostic tool for the early detection of DM. The glycation of albumin proceeds *via* nonenzymatic attachment of glucose residues to the free amino groups of lysine and arginine moieties followed by the formation of Schiff base intermediate, which further undergoes Amadori-rearrangement to form more stable keto-amine or fructosyl-lysine products known as Amadori product (Figure 4A). The glycation of BSA (50 μM) was carried out in the presence of glucose (5 mM) in PBS at 37 °C under continuous incubation for 28 days. Concentration-dependent photophysical studies monitored the extent of glycation of the incubated BSA. The change in emission intensity of tryptophan residue of BSA at 340 nm was recorded upon excitation at 278 nm (Figure 4B). The data showed a decrease in emission intensity at 340 nm in the case of BSA$_G$, which indicates the changes in the tryptophan microenvironment upon glycation. Further, the change in emission intensity in the range of 400–550 nm was measured upon excitation at 370 nm. The characteristic fluorescence signals in the region 400–550 nm are the predictor of the formation of glycated products (Figure S8). The glycation of BSA and the formation of AGEs are accompanied by major structural changes in the protein with globular to β sheet-like conversion.[62]

In this context, the thioflavin-T (ThT) assay is a reliable method to probe the structural changes in BSA$_G$ due to the high affinity of ThT dye towards β sheet-like structures.[28] The assay was performed by treating different concentrations of native BSA or BSA$_G$ (2, 5, and 10 μM) with ThT (10 μM), and the change in emission intensity at 480 nm was recorded upon excitation at 440 nm (Figure S9). There are no significant changes in the ThT fluorescence intensities in the presence of native BSA. While, BSA$_G$ showed a concentration-dependent enhancement in ThT fluorescence intensities, and fluorescence enhancement was significant at 10 μM concentration of BSA$_G$, which revealed alterations in the secondary structure of BSA due to glycation. The structural changes of BSA due to glycation were further confirmed by CD spectroscopy measurement (Figure 4C). The CD spectra of BSA (10 μM) and BSA$_G$ (10 μM) were recorded in PBS. The CD spectrum of native BSA showed characteristic peaks at 205 nm and 225 nm corresponding to the α-helix structure. The CD

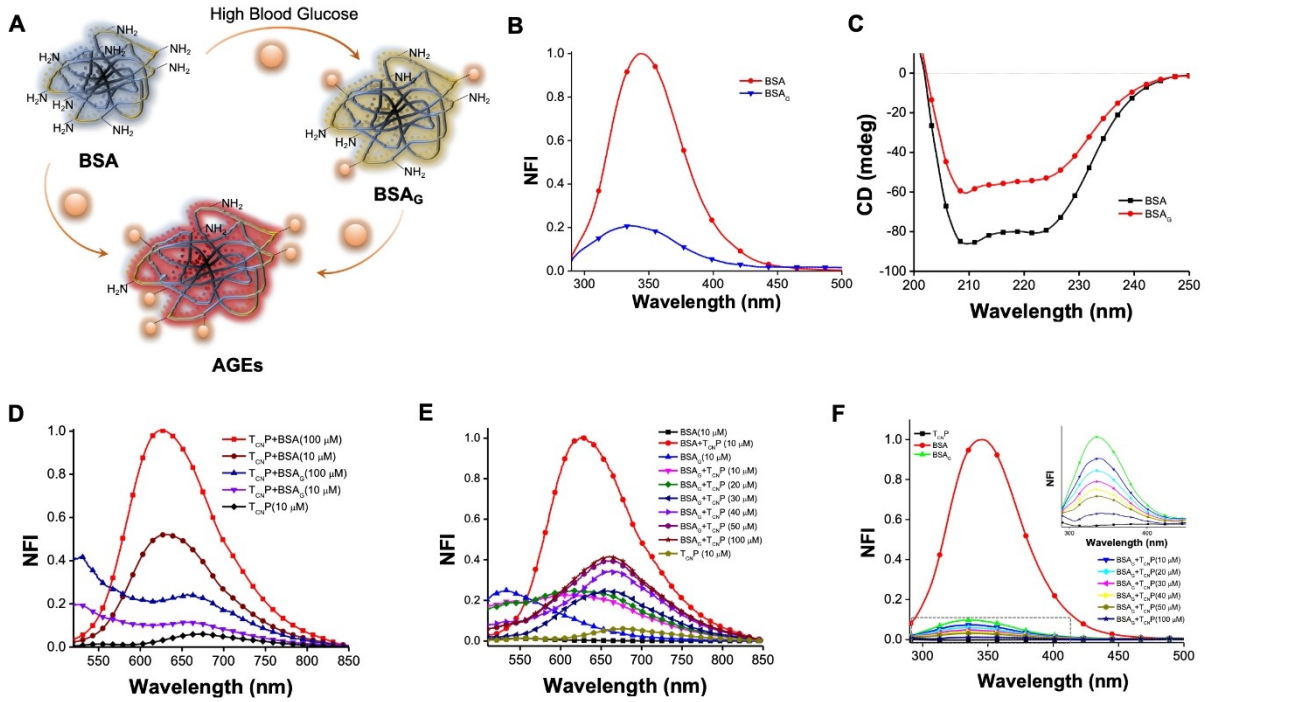

Figure 4. (**A**) Schematic representation of glycation of BSA under high blood glucose levels and the formation of AGEs. (**B**) Intrinsic fluorescence change of BSA upon glycation ($\lambda_{max}=340$ nm, $\lambda_{ex}=278$ nm). (**C**) Circular dichroism (CD) spectra of native BSA and BSA_G confirming the changes in helical content upon glycation. (**D**) The change in fluorescence intensity of $T_{CN}P$ (10 μM) with different concentration of BSA and BSA_G (10 and 100 μM) ($\lambda_{ex}=480$ nm, $\lambda_{em}=656$ nm). (**E**) Intrinsic fluorescence change of BSA_G (10 μM) monitored at 530 nm upon the increasing concentration of the probe (0 to 100 μM) ($\lambda_{ex}=480$ nm, $\lambda_{em}=656$ nm). **(F)** Intrinsic fluorescence change of BSA_G (10 μM) ($\lambda_{ex}=278$ nm, $\lambda_{em}=340$ nm) recorded with increasing concentration of $T_{CN}P$ (0–100 μM). Inset is the enlarged view of the box, which shows changes in intrinsic fluorescence intensity of BSA_G in the presence of varying concentrations of the probe. NFI: Normalized fluorescence intensity.

spectrum of glycated BSA showed a decrease in the peak intensities at 205 nm and 225 nm indicating a reduction in the helical content. This result is in good agreement with ThT fluorescence assay data and confirmed major structural changes to native BSA upon glycation. Next, we performed the matrix-assisted laser desorption and ionization (MALDI) analysis of BSA and BSA_G using 2,5-dihydroxybenzoic acid/sinapinic acid (20 : 80) as the matrix (Figure S10). The MALDI spectrum showed an increased molecular mass peak for glycated BSA compared to native BSA. The increased molecular weight suggests BSA modification upon addition of more than four glucose residues, which subsequently undergo rearrangements to form the glycated derivatives. Next, we investigated the utility of $T_{CN}P$ to differentially probe BSA_G against native BSA. $T_{CN}P$ (10 μM) was treated with native BSA (10 and 100 μM) or BSA_G (10 and 100 μM) and incubated for 15 min at room temperature. The emission spectra of $T_{CN}P$ was recorded upon excitation at 480 nm (Figure 4D). The characteristic enhancement in the emission spectra of $T_{CN}P$ at 619 nm along with hypsochromic shift was unchanged for native BSA. However, significant quenching of fluorescence emission with a bathochromic spectral shifting (~ 55 nm) was observed in the case of BSA_G in comparison to native BSA. Notably, the emission spectra of BSA_G showed a characteristic band at 530 nm (Figure 4E), which is a signature band corresponding to the glycation of arginine units in BSA that unambiguously confirmed the formation of AGEs and Arg-194, Arg-196, Arg-198, Arg-217, Arg-409, Lys-204 and Lys-413 present in sudlow I and sudlow II sites are typically responsible for ligand interaction.[46] The glycation predictably makes significant structural alterations and conformational changes in the sudlow sites due to covalent attachment of glucose units to the amine groups of lysine and arginine residues followed by the cyclic rearrangement to form AGEs. The concentration-dependent study was performed, where the concentration of probe was varied from 10 to 100 μM, and BSA_G concentration was fixed at 10 μM (Figure 4E). The careful observation of the fluorescence data revealed that the characteristic signature band of AGEs at 530 nm was decreased upon interacting with the probe. A subsequent increase in the probe concentration results in the disappearance of the AGE band and reappearance of the intense fluorescence signal at 655 nm, which is gradually enhanced with probe concentration. The glycation-induced modifications of amino acid residues in the drug-binding sites alter the surface area, width, and volume of the binding pockets, which prevents the

probe accessibility and alters the binding interactions. To gain further insights on the probe-analyte interaction, the changes in intrinsic tryptophan fluorescence (λ_{em} = 340 nm, λ_{ex} = 278 nm) was monitored by titrating increasing concentrations of the probe (10 to 100 μM) to a fixed concentration of BSA_G (10 μM). As discussed earlier, the glycation induced structural changes (helix to β-sheet transition) exposes the drug-specific sudlow sites and alters the tryptophan microenvironment of the protein, which reflected in the quenching of tryptophan fluorescence intensity of BSA_G as compared to native BSA (*vide supra*). The observed increased trend in tryptophan fluorescence quenching as a function of probe concentration (10–100 μM) suggests that the probe interaction further contributes to the structural alteration of BSA_G (Figure 4F). The glycation and oxidation induce significant structural alteration to native BSA, which is believed to significantly change the conformation of drug-binding sites (sudlow I and sudlow II). $T_{CN}P$ binds to the hydrophobic drug-binding pocket of native BSA, as revealed by the changes in intrinsic fluorescence signal of protein and turn-on emission of the probe. The conformational changes of BSA upon glycation and oxidation significantly affect the intrinsic protein and probe fluorescence responses, which result in the observed differential detection patterns.

We have developed a fluorescence probe $T_{CN}P$ with a D-π-A molecular system for the differential detection of structural variants of BSA. The detailed photophysical studies performed with $T_{CN}P$ established the selective and differential detection of BSA/HSA, BSA_O, and BSA_G. The photostable $T_{CN}P$ exhibit highly specific turn-on fluorescence emission and distinct photophysical properties in the presence of BSA/HSA and BSA_O, with a maximum enhancement for the latter. The glycation of native BSA resulted in significant conformational changes and showed a prominent fluorescence quenching response in the presence of the probe as compared to other BSA analytes (BSA/HSA or BSA_O). The structural modification of BSA upon oxidation (BSA_O) and glycation (BSA_G) have distinctively influenced the binding interaction of $T_{CN}P$, which resulted in differential fluorescence response. This study underlines the importance of differential detection of structural variants of BSA as the alternative method to blood glucose level measurements for the diagnosis of various pathological conditions. Further, modifications and improvements to the methods and protocols reported here are anticipated to provide novel diagnostic tools for DM and associated disease conditions.

Synthesis of 10-methyl-10H-phenothiazine (1). To a stirred solution of 10H-phenothiazine (500 mg, 2.50 mmol) in DMF in a high-pressure sealed tube, NaH (60 mg, 2.50 mmol) was added at 0 °C. The reaction mixture was stirred for 30 min at 0 °C followed by 15 min at room temperature. To the same solution, MeI (2 mL, 4.55 g, 32.11 mmol) was added dropwise and stirred at 40 °C for 24 h and the reaction was monitored by thin layer chromatography (TLC). After completion of the reaction, the crude reaction mixture was purified by column chromatography on silica gel using ethyl acetate: hexane as eluent to yield a white solid **1** in good yield (60%). ^{1}H NMR (400 MHz, DMSO d_6): δ 7.22 (t, J = 7.7 Hz, 2H), 7.16 (d, J = 7.8 Hz, 2H), 6.96 (dd, J = 7.7 Hz, 4.1 Hz, 4H), 3.31 (s, 3H). ^{13}C NMR (100 MHz, DMSO d_6): δ 145.3, 127.7, 126.7, 122.4, 122.0, 114.5, 35.0. HRMS (ESI) m/z: calcd for $C_{13}H_{11}NS$ $[M+H]^+$, 214.0684; Found, 214.0671.

Synthesis of 10-methyl-10H-phenothiazine-3-carbaldehyde (2). To a stirred solution of **1** (500 mg, 2.34 mmol) in DMF (2 mL), $POCl_3$ (1.5 mL, 1.81 g, 11.83 mmol) was added dropwise under nitrogen atmosphere at 0 °C. The reaction mixture was stirred under the same conditions for 40 min before it was brought to room temperature and stirred for 20 min followed by 3 h at 60 °C and monitored by TLC. After completion of reaction, the reaction mixture was poured into ice-cold water to obtain a yellow-brown precipitate of **2** in good yield (62%). ^{1}H NMR (400 MHz, DMSO d_6): δ 9.80 (s, 1H), 7.75 (d, J = 8.4 Hz, 1H), 7.61 (s, 1H), 7.25 (t, J = 7.7 Hz, 1H), 7.18 (d, J = 7.6 Hz, 1H), 7.10 (d, J = 8.4 Hz, 1H), 7.02 (t, J = 7.4 Hz, 2H), 3.39 (s, 3H). ^{13}C NMR (100 MHz, DMSO d_6): δ 190.6, 150.4, 143.7, 130.9, 130.4, 128.0, 127.2, 126.9, 123.5, 122.4, 121.1, 115.4, 114.5, 35.6. HRMS (ESI) m/z: calcd for $C_{14}H_{11}NOS$ $[M]^+$, 241.0561; found, 241.0967.

Synthesis of 2-(benzothiazole-2-yl)-3-(10-methyl-10H-phenothiazin-3-yl) acrylonitrile ($T_{CN}P$). To a stirred solution of **2** (500 mg, 2.07 mmol) in ethanol (30 mL), piperidine (283 μL, 244 mg, 2.86 mmol) was added dropwise. The reaction mixture was stirred at room temperature for 20 min, to which ethanol solution of 2-(benzo-thiazol-2-yl) acetonitrile (690 mg, 3.96 mmol) was added. The reaction mixture was stirred at room temperature for 24 h and monitored by TLC. After completion of reaction, the reaction mixture was kept at −20 °C overnight for precipitation. The obtained dark-orange precipitate was washed with hexane and purified by column chromatography on silica gel using ethyl acetate: hexane as eluent. The product obtained as an orange solid in excellent yield (80%). ^{1}H NMR (400 MHz, DMSO d_6): δ 8.24 (s, 1H), 8.15 (d, J = 7.9 Hz, 1H), 8.02 (dd, J = 16.9 Hz, 8.4 Hz, 2H), 7.90 (s, 1H), 7.56 (t, J = 7.6 Hz, 1H), 7.49 (t, J = 7.6 Hz, 1H), 7.26 (t, J = 7.7 Hz, 1H), 7.20 (d, J = 7.3 Hz, 1H), 7.13 (d, J = 8.7 Hz, 1H), 7.03 (t, J = 7.5 Hz, 2H), 3.40 (s, 3H). ^{13}C NMR (100 MHz, DMSO d_6): δ 163.5, 152.9, 148.6, 146.4, 143.5, 128.1, 126.9, 123.5, 122.8, 122.3, 115.4, 114.8, 101.8, 35.5. HRMS (ESI) m/z: calcd. for $C_{23}H_{15}N_3S_2$ $[M+H]^+$, 398.0779; found, 398.0837.

BSA Oxidation and Characterization. For the oxidation of BSA, BSA (10 μM) was pretreated with $FeSO_4$ (10 μM) and EDTA (10 μM) in PBS (10 mM, pH = 7.4) for 5 min and then H_2O_2 (100 μM) was added and the sample was incubated for another 10 min at room temperature under dark condition.[63,64] The oxidation of BSA was monitored by cyclic voltammetry (CV) and fluorescence measurements. The samples were purged with argon for 30 min to degas the electrolyte. The cyclic voltammetry was performed in PBS (10 mL, 10 mM, pH = 7.4) using Ag/AgCl (1 M KCl) as a reference electrode, glassy carbon as a working electrode and Pt coil as the counter electrode. The CV spectra were recorded

at a scan rate of 0.1 V/s in the range of −1 V to −0.24 V. The change in the fluorescence intensity was measured at λ_{em} = 340 nm upon excitation at 278 nm.

Glycation of BSA. BSA (50 μM) was incubated with glucose (5 mM) in PBS (10 mM, pH = 7.4) at 37 °C for 28 days under constant agitation.[65] The glycation of BSA was monitored by the change in the fluorescence spectra at λ_{em} = 340 nm upon excitation at 278 nm and λ_{em} = 485 nm upon excitation at 370 nm, respectively, which are the characteristic region to monitor glycation of BSA. After glycation of BSA, the sample was extensively dialyzed in PBS (10 mM, pH = 7.4) using the PVDF membrane (14 kDa) for 48 h to remove excess glucose molecules. The concentration of glycated BSA was measured by Bradford's assay. The stock solutions were stored at −20 °C.

Acknowledgment

We thank JNCASR, SwarnaJayanthi Fellowship grant (DST/SJF/CSA-02/2015-2016), the Department of Science and Technology (DST), India, Sheikh Saqr Laboratory (SSL), ICMS-JNCASR financial support, and CSIR and UGC for student fellowships.

References

[1] C. Bommer, E. Heesemann, V. Sagalova, J. Manne-Goehler, R. Atun, T. Bärnighausen, S. Vollmer, *Lancet Diabetes Endocrinol.* **2017**, *5*, 423–430.
[2] C. C. Patterson, S. Karuranga, P. Salpea, P. Saeedi, G. Dahlquist, G. Soltesz, G. D. Ogle, *Diabetes Res. Clin. Pract.* **2019**, *157*, 107842.
[3] S. Prasad, R. K. Sajja, P. Naik, L. Cucullo, *J. Pharmacovigilance* **2014**, *2*, 125.
[4] M. Bogush, N. A. Heldt, Y. Persidsky, *J. Neuroimmune Pharmacol.* **2017**, *12*, 593–601.
[5] C. Sims-Robinson, B. Kim, A. Rosko, E. L. Feldman, *Nat. Rev. Neurol.* **2010**, *6*, 551–559.
[6] A. M. Vincent, B. C. Callaghan, A. L. Smith, E. L. Feldman, *Nat. Rev. Neurol.* **2011**, *7*, 573–583.
[7] K. Rajasekhar, M. Chakrabarti, T. Govindaraju, *Chem. Commun.* **2015**, *51*, 13434–13450.
[8] H. Arora, M. Ramesh, K. Rajasekhar, T. Govindaraju, *Bull. Chem. Soc. Jpn.* **2020**, *93*, 507–546.
[9] D. Li, Z. Zhang, H. Chang, *Sensors Actuators B: Chem.* **2019**, *291*, 433–440.
[10] T. Kohzuma, M. Koga, *Mol. Diagn. Ther.* **2010**, *14*, 49–51.
[11] K. L. Costa, Z. A. Taboza, G. B. Angelino, V. R. Silveira, R. Montenegro Jr, A. N. Haas, R. O. Rego, *J. Periodontol.* **2017**, *88*, 17–25.
[12] F. K. Yeboah, V. A. Yaylayan, *Food / Nahrung* **2001**, *45*, 164–171.
[13] T. W. Evans, *Aliment. Pharmacol. Ther.* **2002**, *16*, 6–11.
[14] L. G. Naso, L. Lezama, M. Valcarcel, C. Salado, P. Villacé, D. Kortazar, E. G. Ferrer, P. A. M. Williams, *J. Inorg. Biochem.* **2016**, *157*, 80–93.
[15] E. L. Gelamo, C. H. T. P. Silva, H. Imasato, M. Tabak, *Biochim. Biophys. Acta* **2002**, *1594*, 84–99.
[16] T.-T. Zhu, Y. Zhang, X.-A. Luo, S.-Z. Wang, M.-Q. Jia, Z.-X. Chen, *J. Agric. Food Chem.* **2018**, *66*, 1242–1250.
[17] G. J. Quinlan, G. S. Martin, T. W. Evans, *Hepatology* **2005**, *41*, 1211–1219.
[18] R. Dolhofer, H. Wieland, *FEBS Lett.* **1979**, *103*, 282–286.
[19] R. Dolhofer, O. H. Wieland, *Diabetes* **1980**, *29*, 417–422.
[20] I. Sadowska-Bartosz, I. Stefaniuk, S. Galiniak, G. Bartosz, *Redox Biology* **2015**, *6*, 93–99.
[21] S. K. Swain, D. Sarkar, *Appl. Surf. Sci.* **2013**, *286*, 99–103.
[22] S. Chesne, P. Rondeau, S. Armenta, E. Bourdon, *Biochimie* **2006**, *88*, 1467–1477.
[23] D. A. Butterfield, F. Di Domenico, A. M. Swomley, E. Head, M. Perluigi, *Biochem. J.* **2014**, *463*, 177–189.
[24] N. T. Moldogazieva, I. M. Mokhosoev, T. I. Mel'nikova, Y. B. Porozov, A. A. Terentiev, *Oxid. Med. Cell. Longev.* **2019**, *2019*, 3085756.
[25] L. M. Sayre, M. A. Smith, G. Perry, *Curr. Med. Chem.* **2001**, *8*, 721–738.
[26] L. M. Sayre, G. Perry, M. A. Smith, *Chem. Res. Toxicol.* **2008**, *21*, 172–188.
[27] G. Münch, J. Thome, P. Foley, R. Schinzel, P. Riederer, *Brain Res. Rev.* **1997**, *23*, 134–143.
[28] A. Schmitt, J. Schmitt, G. Münch, J. Gasic-Milencovic, *Anal. Biochem.* **2005**, *338*, 201–215.
[29] E. Schleicher, O. H. Wieland, *J. Clin. Chem. Clin. Biochem.* **1989**, *27*, 577–587.
[30] M. Rendell, K. Rasbold, J. Nierenberg, R. Krohn, G. Hermanson, D. Klenk, P. K. Smith, *Clin. Biochem.* **1986**, *19*, 216–220.
[31] H. Ki, J. Oh, G.-R. Han, M.-G. Kim, *Lab Chip* **2020**, *20*, 844–851.
[32] T. Kouzuma, T. Usami, M. Yamakoshi, M. Takahashi, S. Imamura, *Clin. Chim. Acta* **2002**, *324*, 61–71.
[33] Y. Inoue, M. Inoue, M. Saito, H. Yoshikawa, E. Tamiya, *Anal. Chem.* **2017**, *89*, 5909–5915.
[34] L. Unger-Angel, B. Rout, T. Ilani, M. Eisenstein, L. Motiei, D. Margulies, *Chem. Sci.* **2015**, *6*, 5419–5425.
[35] L. Yuan, W. Lin, K. Zheng, L. He, W. Huang, *Chem. Soc. Rev.* **2013**, *42*, 622–661.
[36] K. Rajasekhar, C. J. Achar, T. Govindaraju, *Org. Biomol. Chem.* **2017**, *15*, 1584–1588.
[37] Y. V. Suseela, N. Narayanaswamy, S. Pratihar, T. Govindaraju, *Chem. Soc. Rev.* **2018**, *47*, 1098–1131.
[38] K. Rajasekhar, N. Narayanaswamy, N. A. Murugan, K. Viccaro, H. G. Lee, K. Shah, T. Govindaraju, *Biosens. Bioelectron.* **2017**, *98*, 54–61.
[39] K. Rajasekhar, N. Narayanaswamy, N. A. Murugan, G. Kuang, H. Ågren, T. Govindaraju, *Sci. Rep.* **2016**, *6*, 23668.
[40] N. Narayanaswamy, S. Narra, R. R. Nair, D. K. Saini, P. Kondaiah, T. Govindaraju, *Chem. Sci.* **2016**, *7*, 2832–2841.
[41] D. Maity, A. Raj, P. K. Samanta, D. Karthigeyan, T. K. Kundu, S. K. Pati, T. Govindaraju, *RSC Adv.* **2014**, *4*, 11147–11151.
[42] N. Narayanaswamy, M. Kumar, S. Das, R. Sharma, P. K. Samanta, S. K. Pati, S. K. Dhar, T. K. Kundu, T. Govindaraju, *Sci. Rep.* **2014**, *4*, 6476.
[43] D. Maity, T. Govindaraju, *Org. Biomol. Chem.* **2013**, *11*, 2098–2104.
[44] N. Narayanaswamy, S. Das, P. K. Samanta, K. Banu, G. P. Sharma, N. Mondal, S. K. Dhar, S. K. Pati, T. Govindaraju, *Nucleic Acids Res.* **2015**, *43*, 8651–8663.
[45] D. Maity, A. Raj, D. Karthigeyan, T. K. Kundu, T. Govindaraju, *Supramol. Chem.* **2015**, *27*, 589–594.

[46] D. Maity, A. K. Manna, D. Karthigeyan, T. K. Kundu, S. K. Pati, T. Govindaraju, *Chem. Eur. J.* **2011**, *17*, 11152–11161.
[47] S. Lee, D.-B. Sung, S. Kang, S. Parameswaran, J.-H. Choi, J. S. Lee, M. S. Han, *Sensors (Basel)* **2019**, *19*, 5298.
[48] C. Liu, W. Yang, Q. Gao, J. Du, H. Luo, Y. Liu, C. Yang, *J. Lumin.* **2018**, *197*, 193–199.
[49] J. Baraka-Vidot, A. Guerin-Dubourg, E. Bourdon, P. Rondeau, *Biochimie* **2012**, *94*, 1960–1967.
[50] S. Awasthi, N. A. Murugan, N. T. Saraswathi, *Mol. Pharm.* **2015**, *12*, 3312–3322.
[51] N. I. Shank, K. J. Zanotti, F. Lanni, P. B. Berget, B. A. Armitage, *J. Am. Chem. Soc.* **2009**, *131*, 12960–12969.
[52] T. Chen, Z. Chen, R. Liu, S. Zheng, *Org. Biomol. Chem.* **2019**, *17*, 6398–6403.
[53] A. Toutchkine, D. V. Nguyen, K. M. Hahn, *Org. Lett.* **2007**, *9*, 2775–2777.
[54] S. Samanta, T. Govindaraju, *ACS Chem. Neurosci.* **2019**, *10*, 4847–4853.
[55] N. Narayanaswamy, S. Das, P. K. Samanta, K. Banu, G. P. Sharma, N. Mondal, S. K. Dhar, S. K. Pati, T. Govindaraju, *Nucleic Acids Res.* **2015**, *43*, 8651–8663.
[56] B. Bagchi, D. W. Oxtoby, G. R. Fleming, *Chem. Phys.* **1984**, *86*, 257–267.
[57] G. Sudlow, D. J. Birkett, D. N. Wade, *Mol. Pharmacol.* **1975**, *11*, 824–832.
[58] G. Sudlow, D. J. Birkett, D. N. Wade, *Mol. Pharmacol.* **1976**, *12*, 1052–1061.
[59] R. Joshi, M. Jadhao, H. Kumar, S. K. Ghosh, *Bioorg. Chem.* **2017**, *75*, 332–346.
[60] R. Misra, S. Kar, *Chem. Phys.* **2012**, *397*, 65–73.
[61] Z. Turk, S. Ljubic, N. Turk, B. Benko, *Clin. Chim. Acta* **2001**, *303*, 105–115.
[62] B. Bouma, L. M. Kroon-Batenburg, Y.-P. Wu, B. Brünjes, G. Posthuma, O. Kranenburg, P. G. de Groot, E. E. Voest, M. F. Gebbink, *J. Biol. Chem.* **2003**, *278*, 41810–41819.
[63] S. Guedes, R. Vitoriro, R. Domingues, F. Amado, P. Domingues, *Rapid Commun. Mass Spectrom.* **2009**, *23*, 2307–2315.
[64] C. P. Baron, H. E. F. Retsgaard, L. H. Skibsted, M. L. Andersen, *Free Radical Res.* **2006**, *40*, 409–417.
[65] A. Schmitt, J. Schmittb, G. Münchc, J. Gasic-Milencovica, *Anal. Biochem.* **2005**, *338* 201–215.

Manuscript received: November 11, 2020
Revised manuscript received: January 11, 2021
Version of record online: January 26, 2021